Analysis of Thin Plates by the Element-Free Galerkin Method

Petr Krysl and Ted Belytschko*

October 7, 1999

Abstract

A meshless approach to the analysis of arbitrary Kirchhoff plates by the Element-Free Galerkin (EFG) method is presented. The method is based on moving least squares approximant. The method is meshless, which means that the discretization is independent of the geometric subdivision into "finite elements". The satisfaction of the C^1 continuity requirements are easily met by EFG since it requires only C^1 weights; therefore, it is not necessary to resort to Mindlin-Reissner theory or to devices such as discrete Kirchhoff theory. The requirements of consistency are met by the use of a quadratic polynomial basis. A subdivision similar to finite elements is used to provide a background mesh for numerical integration. The essential boundary conditions are enforced by Lagrange multipliers. It is shown, that high accuracy can be achieved for arbitrary grid geometries, for clamped and simply-supported edge conditions, and for regular and irregular grids. Numerical studies are presented which show that the optimal support is about 3.9 node spacings, and that high-order quadrature is required.

1 Introduction

There is a growing interest in the so-called "meshless" methods. It might be partly traced to high costs involved in meshing procedures. Modelling of adapting domain geometry, fracture, fragmentation and similar phenomena requires considerable remeshing efforts, which can easily constitute the largest portion of analysis costs.

Meshless methods do not require a finite element mesh. The discretization is based on a set of nodes (ordered or scattered). The connectivity in terms of node interactions may be changing constantly, and modelling of fracture, free surfaces, large deformations, etc. is considerably simplified – *cf.* Belytschko *et al.* (1994) [1].

*Department of Civil Engineering, Robert R. McCormick School of Engineering and Applied Science, The Technological Institute, Northwestern University, Evanston, IL 60208-3109, U.S.A.

Meshless methods have been proposed in several varieties as Generalized Finite Difference Method (Liszka (1984) [14]), Smoothed Particle Hydrodynamics (Monaghan (1982) [17]), Diffuse Element Method (Nayroles (1992) [18]), Wavelet Galerkin Method (e.g. Qian and Weiss (1993) [19]), Multiquadrics (Kansa (1990) [10, 11]), Reproducing Kernel Particle Methods (Liu *et al.* (1995) [15]) and the Element-Free Galerkin Method (Belytschko *et al.* (1994) [2]).

The Element-Free Galerkin Method (EFGM) is based on a moving least squares approximation. These approximations originated in scattered data fitting, where it has been studied under different names (local regression, "loess", and moving least squares) since the 1920's – *cf.* Cleveland (1993) [6] and Lancaster and Šalkauskas (1986) [13].

The enforcement of essential boundary conditions in the EFGM requires special treatment, therefore a number of techniques have been proposed such as point collocation, Lagrange multipliers, and coupling with finite elements. The coupling with finite element methods seems especially desirable as the computational costs are relatively high for the EFG method due to its dynamic connectivity character (the connectivity, i.e. the interaction of nodes, is not fixed by input data, it needs to be computed).

The goal of the present paper is to develop the EFG method for problems of thin plate bending – usually denoted as Kirchhoff plates. The problem of constructing C^1 finite elements for plate bending of general shape (i.e. not just rectangles) has been addressed by many researchers. Although C^1 elements have been developed, alternative methodologies which circumvent the continuity requirement seem to have taken over in recent years. The most popular are the discrete Kirchhoff theory, and the hybrid and mixed models.

The EFG method offers considerable potential with respect to numerical solutions of boundary-value problems that require high continuity in the trial functions – Kirchhoff plate theory being one of them. The continuity of the shape functions is primarily governed by the continuity of the weight function. Therefore, as it is possible to construct sufficiently smooth weight functions, the numerical approach is greatly simplified.

The outline of the paper is as follows: First, a very short account of the numerical formulation of the Kirchhoff plate theory is given. The EFG method approximation is then reviewed: the moving least squares technique, the properties of the EFG approximation, and the construction of the shape functions. The discretization issues are then discussed: numerical integration on a background mesh, computation of the stiffness matrix, and the enforcement of the essential boundary conditions. A discussion of the choice of the weight function then follows, with some comments on the way in which the choice of the weight function support affects the solution.

The paper is concluded by a section on numerical experiments. The well-known plate benchmarks, the square and circular plate under various loads, are explored. The dependence of the solutions on the quadrature order, on the support size and on grid irregularity is investigated, and conclusions are drawn with respect to recommended or "optimal" choices.

2 Governing equations

A standard Kirchhoff formulation of the plate equation, which results in a biharmonic equation in the transverse displacement, is used. Because of the occurrence of 4^{th} order partial derivatives in the governing equation, C^1 approximations are needed. The equations are written in a cartesian system with the basis vector $\boldsymbol{E}_3$ normal to the plate. The displacement along the z axis is denoted u_z.

The principle of virtual work is written as

$$\delta W(\delta u_z) = \int_{\mathcal{A}} m^{\beta\alpha}\delta\kappa_{\beta\alpha}\ \mathrm{d}\mathcal{A} - \delta W_{ext}(\delta u_z)\ , \tag{2.1}$$

with $W_{ext}(\delta u_z)$ as the virtual work of the external loading

$$\delta W_{ext}(\delta u_z) = \int_{\mathcal{A}} [\bar{p}\delta u_z + \bar{m}_\alpha \delta t_\alpha]\ \mathrm{d}\mathcal{A} + \int_{\partial_q\mathcal{A}} \bar{q}\delta u_z\ \mathrm{d}s + \int_{\partial_m\mathcal{A}} \bar{m}_{(\tau)}\delta t_{(\tau)}\ \mathrm{d}s \tag{2.2}$$

where the u_z is the plate deflection (along z axis), $\bar{p}$ is the prescribed distributed load per unit area normal to the plate, $\bar{q}$ is the prescribed distributed shear per unit boundary curve length, $\bar{m}_\alpha \boldsymbol{E}_\alpha$ is the prescribed distributed moment per unit area, $\bar{m}_{(\tau)}$ is the distributed moment along the boundary curve (there is no summation over τ in the above equation), and $\boldsymbol{t} \equiv \boldsymbol{E}_3$ is the unit vector normal to the plate reference surface. The symbols $\mathcal{A}$, $\partial_q\mathcal{A}$ and $\partial_m\mathcal{A}$ denote the plate domain, and its boundary with prescribed shear and moments, respectively.

The curvatures are defined as

$$\kappa_{11} = -u_{z,xx}\ ,\ \kappa_{22} = -u_{z,yy}\ ,\ \kappa_{12} = \kappa_{21} = -u_{z,xy}\ . \tag{2.3}$$

Arranging the moments and the curvatures in vectors, we can write the isotropic elastic constitutive equation as

$$\left\{ \begin{array}{c} m^{11} \\ m^{22} \\ m^{12} \end{array} \right\} = D\boldsymbol{C} \left\{ \begin{array}{c} \kappa^{11} \\ \kappa^{22} \\ 2\kappa^{12} \end{array} \right\} \tag{2.4}$$

with the isotropic elasticity matrix $\boldsymbol{C}$

$$\boldsymbol{C} = \left[\begin{array}{ccc} 1 & \nu & 0 \\ \nu & 1 & 0 \\ 0 & 0 & \frac{1}{2}(1-\nu) \end{array} \right]\ , \tag{2.5}$$

and with the flexural rigidity D being given as (E is the Young's modulus, ν is the Poisson constant, and t is the plate thickness)

$$D = \frac{Et^3}{12(1-\nu^2)}\ . \tag{2.6}$$

3 Domain description

The Element-Free Galerkin method uses the moving least-squares approximation (MLS) to construct the numerical discretization. The MLS have been used in statistics under the name of "loess" (local regression) to fit curves or surfaces to scattered data since the 1920's – *cf.* details in [6] and references therein.

3.1 Moving Least Squares

The starting point of the Element-Free Galerkin method (EFGM) is the following equation, which approximates a function $u(\boldsymbol{x})$ in a small neighbourhood of $\boldsymbol{x}$ by a (seemingly) polynomial expansion (actually, the approximation is much more complicated; for instance, it is rational when a a polynomial weight function is used):

$$u(\boldsymbol{x}) = p_j(\boldsymbol{x}) a_j(\boldsymbol{x}) \ , \quad j = 1, \ldots, n \tag{3.1}$$

The polynomial basis $p_j(\boldsymbol{x})$ is known, the unknown coefficients $a_j(\boldsymbol{x})$ are solved for by the moving least-squares procedure using prescribed values u_I at nodal points $\boldsymbol{x}_I$, $I = 1, \ldots, M$. As is well known, the approximation (3.1) *must be at least quadratic* when applied to fourth-order problems (see e.g. Strang and Fix' book [20]). The reason is, that the governing weak form contains second-order derivatives, so that a quadratic polynomial must be represented exactly by (3.1), for the purpose of consistency. Although equation (3.1) is in general of degree higher than that of $p_j(\boldsymbol{x})$, the above requirement will hold for the choice $a_j(\boldsymbol{x}) = const.$ Consequently, the MLS approximation with a quadratic basis will represent a quadratic polynomial exactly. The polynomial basis adopted in this work is

$$\{p_j(\boldsymbol{x})\}^T = \left\{1, x, y, x^2, xy, y^2\right\}^T , \quad \text{with } n = 6 \ . \tag{3.2}$$

Note, that for the actual calculations, the argument $\boldsymbol{x}$ should be replaced by simple linear transformation $\bar{\boldsymbol{x}} = \boldsymbol{x} - \boldsymbol{x}_{orig}$ to shift the origin to the evaluation point. Otherwise, a loss of accuracy follows from the absolute values of $\boldsymbol{x}$ being too large.

The moving least-squares technique consists in minimizing the weighted L_2 norm

$$J = \sum_{I=1}^{M} w(\boldsymbol{x} - \boldsymbol{x}_I) \left[p_j(\boldsymbol{x}_I) a_j(\boldsymbol{x}) - u_I\right]^2 \ , \tag{3.3}$$

where $w(\boldsymbol{x} - \boldsymbol{x}_i)$ is a weight function of compact support (often called the domain of influence of node i).

This yields the following linear system of equations for the coefficients a_j:

$$\boldsymbol{A}(\boldsymbol{x}) \{a_j\} = \boldsymbol{B}(\boldsymbol{x}) \{u_m\} \ , \qquad \{a_j\} \in R^n, \{u_m\} \in R^M \tag{3.4}$$

where M is the number of EFG nodes whose domain of influence includes $\boldsymbol{x}$, and

$$\left[\boldsymbol{A}(\boldsymbol{x})\right]_{ij} = \sum_{m=1}^{M} w(\boldsymbol{x} - \boldsymbol{x}_m) p_i(\boldsymbol{x}_m) p_j(\boldsymbol{x}_m) \ ,$$

$$\boldsymbol{B}(\boldsymbol{x}) = \left[w(\boldsymbol{x}-\boldsymbol{x}_1)\left\{p_i(\boldsymbol{x}_1)\right\}, \ldots, w(\boldsymbol{x}-\boldsymbol{x}_M)\left\{p_i(\boldsymbol{x}_M)\right\}\right] \ .$$

The equation (3.1) can thus be put into standard form

$$u(\boldsymbol{x}) = \left\{\phi_I(\boldsymbol{x})\right\}^T \left\{u_I\right\} \ , \qquad \left\{\phi_I\right\} \in R^M, \left\{u_I\right\} \in R^M \ , \tag{3.5}$$

with $\phi_I(\boldsymbol{x})$ being the *shape functions*

$$\phi_I(\boldsymbol{x}) = p_j \left[\boldsymbol{A}(\boldsymbol{x})^{-1} \cdot \boldsymbol{B}(\boldsymbol{x})\right]_{jI} \ . \tag{3.6}$$

The continuity of the shape function $\phi_I(\boldsymbol{x})$ is governed by the continuity of the basis functions p_j, and by the smoothness of the matrices $\boldsymbol{A}(\boldsymbol{x})^{-1}$ and $\boldsymbol{B}(\boldsymbol{x})$. The latter is governed on the smoothness of the weight function.

3.2 Description of the plate domain

The plate domain can be described in terms of its boundary. The crucial issue in a numerical procedure is the numerical integration. It can be carried out in a system of background cells as e.g. in [2], or a finite element mesh (or similar geometric subdivision) can be used as indicated below.

3.2.1 Background mesh

The background mesh is simply a subdivision of the plate domain into distinct, non-overlapping, simple shapes like triangles, quadrangles etc. such that the plate domain is a union of these shapes. The geometric subdivision needs not be a valid finite element mesh at all. In particular, there may be arbitrary incompatibility in the mesh in that vertices need not be shared by adjacent elements – *cf.* figure 1. Note, that the subdivision into elements need not be in any way related to the distribution of the EFG nodes, although it might be convenient to place EFG points at the vertices of the background elements.

REMARK 1: The use of a finite element mesh for the purpose of shape definition/ numerical integration seems to be of value also with respect to coupling with the finite element technique – *cf.* Belytschko *et al.* [3]. In that case, the finite element mesh would be readily available without additional cost.

4 Approximation of the displacements

The displacement $u_z(\boldsymbol{\xi})$ will be approximated by a simple variant of the equation (3.1)

$$u_z(\boldsymbol{\xi}) = \sum_{I=1}^{M} \phi_I(\boldsymbol{\xi}) U_{zI} \ . \tag{4.1}$$

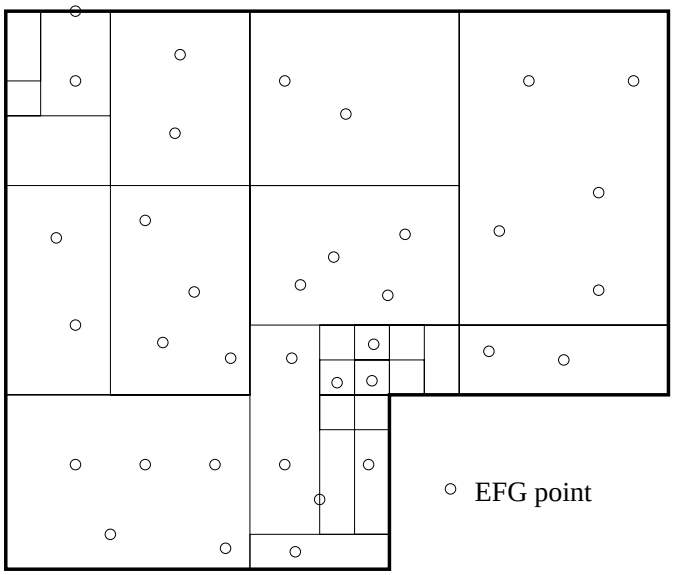

Figure 1: Sample geometric subdivision of an L-shaped plate domain into simple shapes ("finite elements").

Note, that U_{zI} are the nodal parameters, but not the nodal deflections. The deflections at the EFG nodes must be computed using (4.1).

To be able to write the weak form (2.1) the first and second order partial derivatives of the shape functions need to be computed. The evaluation of these derivatives constitutes a major cost factor.

5 Stiffness matrix

It should be noted, that one of the characteristic features of the EFG method is the variable number of nodal points affecting an integration point. Therefore, it is convenient to write the strain-displacement matrices in a symbolic form as a sum of submatrices (one for each EFG node, whose support interferes with the integration point in question), rather than as a matrix with variable number of columns.

The curvatures at an integration point $\boldsymbol{x}_Q$ can be put down as a sum over all EFG nodes whose support includes the point $\boldsymbol{x}_Q$

$$\{\kappa\} = \{B_I(\boldsymbol{x}_Q)\}\, U_{zI} \ , \tag{5.1}$$

where the strain-displacement submatrices $\{B_I(\boldsymbol{x}_Q)\}$ are reduced to vectors, which are multiplied by the scalars U_{zI}. The strain-displacement submatrix can be detailed as

$$\{B_I\} = \left\{ \begin{array}{c} -\phi_{I,xx} \\ -\phi_{I,yy} \\ -2\phi_{I,xy} \end{array} \right\} \ . \tag{5.2}$$

Consequently, the stiffness matrix can be computed by evaluating and assembling at each integration point the following integral

$$\int_{\mathcal{A}} D \left\{B_I\right\}^T \boldsymbol{C} \left\{B_K\right\} \, \mathrm{d}\mathcal{A} \, . \tag{5.3}$$

6 Essential boundary conditions

An Element-Free Galerkin handling of essential boundary conditions (EBC) is awkward as the shape functions do not vanish on the boundary of the domain (*cf.* the reference [16]). Some of the options are: (i) point collocation [8], (ii) Lagrange multipliers [2], (iii) modified Lagrange multipliers (replacement of multipliers by their physical representations in terms of reaction forces, see [16]), (iv) enforcement by finite elements at the boundary [12]. The technique (i) lacks precision, therefore it was not considered here. Approach (iii) is not attractive for Kirchhoff-Love theory, as third-order derivatives of the shape functions are needed to compute the effective forces on the boundary, and these are expensive to compute and not very accurate. The technique ad (iv) seems to be advantageous, it was not yet tested with the plates, however.

The approach selected here to enforce the essential boundary conditions is the method of Lagrange multipliers (technique ad (ii)). The disadvantages (unpleasant, but not prohibitive) are:

- Additional unknowns increase the problem size.
- Special solver is needed to handle the resulting indefinite system of linear equations with a structure that resembles that of mixed finite element methods. (Bunch-Kauffman-Parlett symmetric indefinite factorization as described in [4] was used here.)

The essential boundary conditions are assumed to be enforced at the boundary of the plate or along any curve crossing the plate domain. There are two species of Lagrange multipliers in the plate problem which are associated with: (a) transverse displacement, (b) rotation about the tangent to the boundary.

The displacement condition is easy to write down, so we concentrate on the rotation about the tangent vector. The component θ_τ of the rotation about the tangent vector $\boldsymbol{\tau}^0$ is obtained readily as $\theta_\tau = \boldsymbol{\theta} \cdot \boldsymbol{\tau}^0$. The small rotation vector can be expressed from the obvious approximation of the increment of the normal vector

$$\Delta \boldsymbol{t} = \boldsymbol{t} - \boldsymbol{t}^0 \approx \boldsymbol{\theta} \times \boldsymbol{t}^0 \, , \tag{6.1}$$

where $\boldsymbol{\theta}$ is the small-rotation vector. The rotation vector $\boldsymbol{\theta}$ can be written as

$$\boldsymbol{\theta} = \left(\phi_{I,y} \boldsymbol{E}_1 - \phi_{I,x} \boldsymbol{E}_2\right) U_{zI} \, . \tag{6.2}$$

The terms corresponding to prescribed rotations about the tangent to the curve $\partial_u \mathcal{A}$, which actually appear in the augmented weak form of (2.1) are now easily detailed as

$$-\int_{\partial_m \mathcal{A}} \delta\lambda_\tau \left(\theta_\tau - \bar{\theta}_\tau\right) \, \mathrm{d}s - \int_{\partial_m \mathcal{A}} \delta\theta_\tau \lambda_\tau \, \mathrm{d}s \tag{6.3}$$

7 Weight function

The EFG method leads to a "parameterized" formulation of the discrete problem, where the parameters are the sizes of the domains of influence of the EFG points. These domains can be of any shape, but circles are the most common ones (i.e. isotropic weight functions). The radius of the support circle of the I^{th} point is given by the definition of the weight function. The weight function needs to be

$$\begin{array}{ll} \text{(i)} & \text{non-negative, and} \\ \text{(ii)} & \text{it must hold that} \quad w_I(\boldsymbol{\xi}) = w(\|\boldsymbol{\xi} - \boldsymbol{\xi}_I\|, R_I) \ , \end{array} \tag{7.1}$$

where R_I is the radius of the support of the I^{th} node.

The EFG method has been in the meantime presented with a variety of weight functions. The weight function chosen for the Kirchhoff-Love shells is the quartic spline because of the continuity of the function and of its derivatives. The spline can be put down as a function of the normalized distance r

$$w(r) = \begin{cases} (1 - 6r^2 + 8r^3 - 3r^4) & \text{for } 1 > r \geq 0, \\ 0 & \text{for } r \geq 1. \end{cases} \tag{7.2}$$

with the normalized distance r being

$$r = \frac{\|\boldsymbol{\xi} - \boldsymbol{\xi}_I\|\cdot}{R_I} \ . \tag{7.3}$$

The support radius could be computed from the arrangement of the EFG points within the domain, for instance by requiring the domain of an EFG point to include a certain number of adjacent EFG points.

The radius of the support domain affects the solution. It is in this manner, that the term "parameterized discrete problem" is to be understood. The size of the support can be arbitrary, provided that it is large enough to yield a regular matrix $\boldsymbol{A}(\boldsymbol{x})$ of equation (3.4). It must include sufficiently large number of EFG points – at least 6 points for quadratic basis p_j – which must not be located in a special pattern (conic section for quadratic basis). Consequently, there emerges the question whether there is an "optimal" support radius, and how to compute it. The issue was investigated further in the section on numerical examples below. Let us just note here, that the larger the support domain, the higher order the approximation achieved (by including larger number of EFG points). There is a limit to it, however. Consider a weight

function radius approaching infinity. The moving least squares approximant then degenerates to standard quadratic least squares scheme. Increasing the domain of influence also makes the computation more costly. Therefore, the task of finding an optimal support radius could be complicated further by introducing a cost function.

8 Numerical examples

8.1 Discretization

The discretizations of the examples considered in this section were constructed in the following manner: Geometric subdivisions of the domains in the form of quadrilaterals were used to define the plate domain. The EFG points were generated at the vertices of these quadrilaterals. This is in no way a restriction of the algorithm, it is merely a convenience, and an effort to "optimize" performance – it seems of advantage to have EFG points at the corners of the domain. Otherwise the choice was arbitrary.

The grids were either regular (orthogonal nets), or irregular. The irregular grids were generated by first triangulating the domain, and then splitting the triangles into three quadrilaterals by connecting the triangle barycenter to the mid-points of its edges.

The support domains of all the EFG points were the same, so that we have that $R_I = R$. Let us define a parameter κ given by

$$\kappa = \frac{R}{h} \ , \tag{8.1}$$

with R being the support radius (radius of the circle in which the shape function associated to an EFG node is non-zero), and h is the "mesh" size. The mesh size is for regular rectangular grids identical to the length of the longer side of the quadrature domain. In cases where the quadrature domains are of different shape, the mesh size h will be explicitly defined. To help in the interpretation of the results, figure 2 presents an overview of the values of the parameter κ for regular grid composed of square integration domains with respect to the number of EFg points included in the circle of radius R (the EFG nodes are located at the vertices of the grid).

The numerical quadrature was performed on the quadrilaterals by $N_G \times N_G$ Gaussian integration. The quadrature order N_G was established by numerical experiment described in section 8.3.

The essential boundary conditions have been enforced by the Lagrange multiplier method. The Lagrange multipliers were defined at the locations of the EFG points on the boundary. Linear interpolation was used on the boundary between the EFG points. One-point quadrature has been applied on the spans.

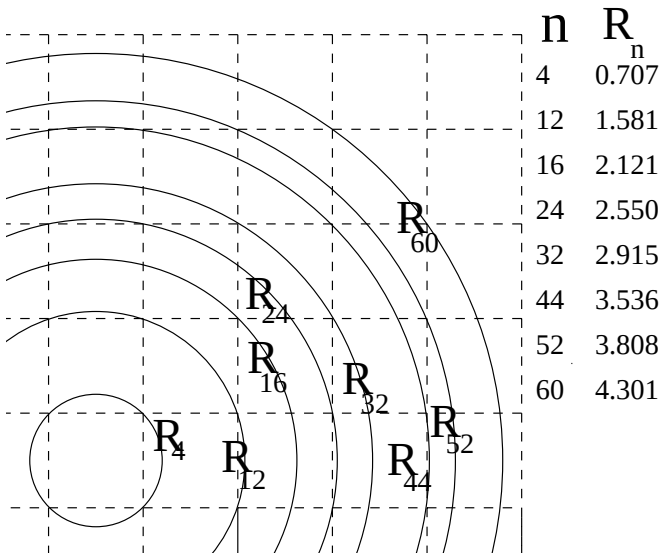

Figure 2: Values of parameter κ on a regular grid (square integration domains) for circles holding 4, 12, 16, 24, 32, 44, 52, and 60 EFG points.

8.2 Square plate

The square plate under various loads is a well-known benchmark with a large number of numerical and analytical solutions to compare with. The present results were compared with some representatives of high-performance finite elements for Kirchhoff plates. Two setups were analyzed:

- Simply-supported plate with concentrated central force. The center deflection as given by Timoshenko [21] of $u_z = 0.0116Pa^2/D$ has been used to normalize the numerical results.
- Clamped plate with concentrated central force. The center deflection as given by Timoshenko [21] of $u_z = 0.0056Pa^2/D$ has been used to normalize the numerical results.

The meanings of the above symbols are: P is the force, a is the (full) plate side length, D is the flexural rigidity of equation (2.6), E is the elastic modulus, ν is the Poisson ratio, and h is the plate thickness.

8.3 Dependence on the quadrature order

Numerical experiments were conducted for quadrature schemes up to 9×9 integration points for both the simply-supported and clamped plate in two models, a full plate model and a quarter plate with appropriate symmetry boundary conditions. The quadrature schemes and the parameter κ were varied.

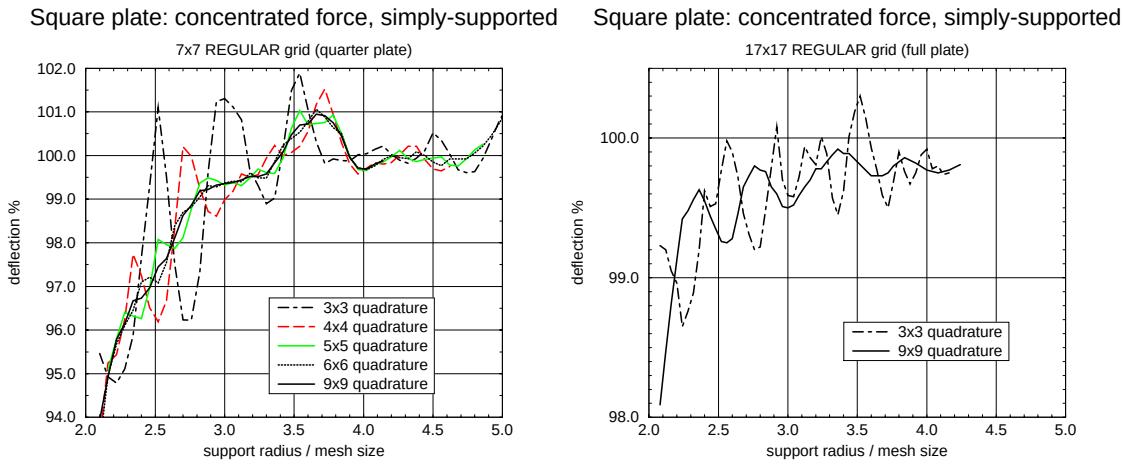

(a) 7×7 grid on quarter plate.

(b) 17×17 grid on full plate.

Figure 3: Deflection of the simply-supported square plate with central force. Results for different quadrature schemes.

8.3.1 Simply-supported plate

The results were summarized in figure 3 for the 7×7 grid on the quarter plate model, and for 17×17 grid on the full model.

8.3.2 Clamped plate

The results were summarized in figure 4 the 7×7 grid on the quarter plate model, and for 17×17 grid on the full model.

8.3.3 Optimal quadrature

To assess the optimal quadrature order rigorously seems rather difficult undertaking. Therefore, to gain insight, a numerical approach based on comparison of results obtained, (a) for tested quadrature scheme, and (b) for very high-order quadrature scheme, has been adopted here. The results seem to indicate that the 6×6 quadrature scheme is close to optimal in that (i) it is not excessively expensive, and (ii) the difference between results obtained for the 6×6 and for the 9×9 quadrature can be viewed as negligible (the 9×9 quadrature being considered "converged").

8.4 Influence of the support radius

Curves of figures 3 and 4 suggest that there exist a number of "higher" accuracy values of the parameter κ (defined in (8.1)). To make it easier to compare the different solutions in depence on the parameter κ (*cf.* (8.1)), the curves for 6×6 quadrature have been collected in figure 5.

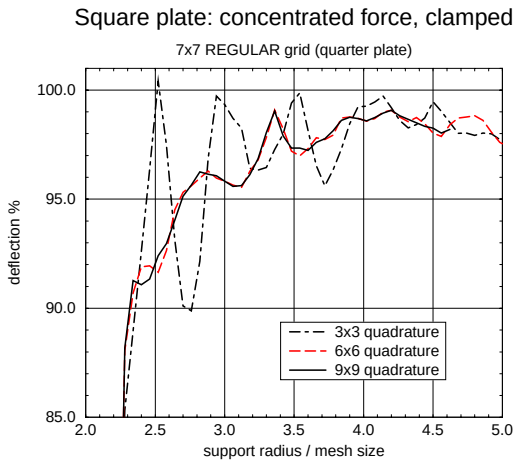

(a) 7×7 grid on quarter plate.

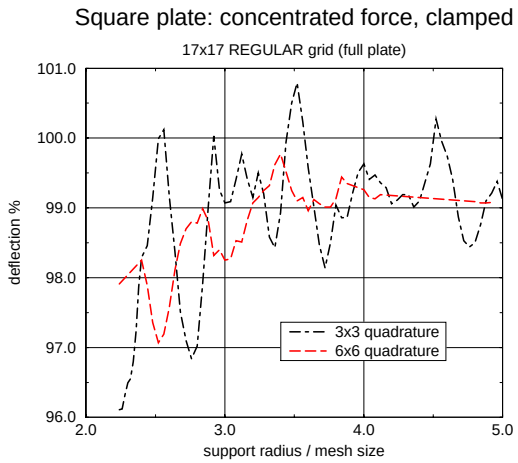

(b) 17×17 grid on full plate.

Figure 4: Deflection of the clamped square plate with central force. Results for different quadrature schemes.

The values $\kappa \approx 3.4$ and $\kappa \approx 3.9$ give in all cases (with the exception of the grid 5×5 which does not contain enough EFG points, to achieve sufficiently high order of the approximation) sequences of lower-error solutions for diminishing mesh size, with $\kappa \approx 3.9$ being more the accurate one for irregular grids and for the symmetry-reduced models. It should be noted, that the number of EFG points contained within the support domains is relatively high (*cf.* figure 2).

8.5 Influence of grid irregularity

The irregular grids tend to perform worse than the regular ones. This is also a characteristic of the finite element method. The EFG method shows much less pronounced loss of accuracy, and what is even more important, increase in support radius (and the associated increase in approximation order) leads to improved accuracy even for irregular grids.

One of the analyzed irregular EFG grids is reproduced in figure 6 (for 7 EFG nodes along half the plate side). Dependence of the deflections of the simply-supported plate on the parameter κ were graphed in figure 7, and figure 8 depicts this relationship for the clamped plate. It should be noted, that the higher accuracy of the parameter κ can be discerned at slightly different locations than for the regular grids. The irregular discretizations give for $\kappa \approx 3.9$ results which compare very favourably with those obtained for regular grids.

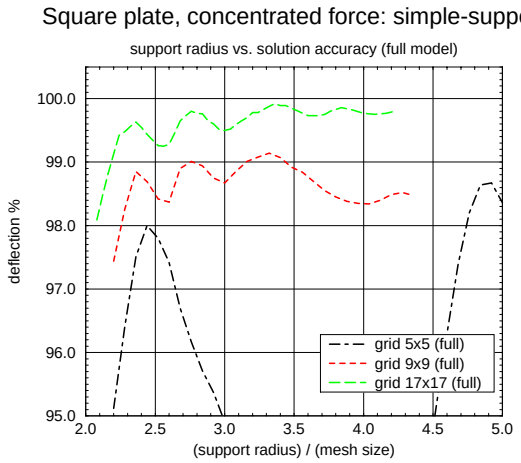

(a) Simply-supported plate. Full model.

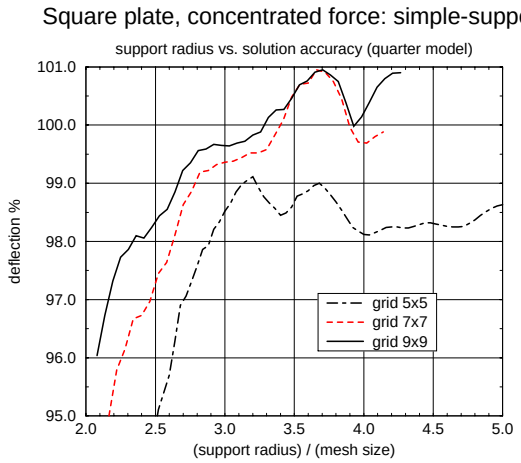

(b) Simply-supported plate. Quarter model.

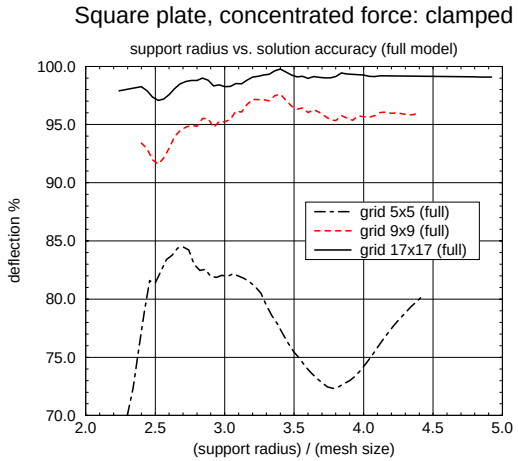

(c) Clamped plate. Full model.

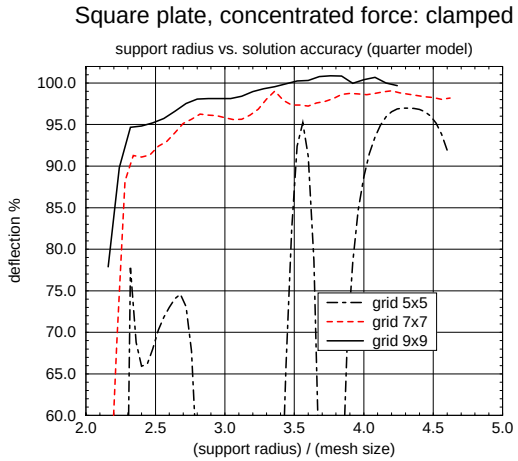

(d) Clamped plate. Quarter model.

Figure 5: Dependency of the deflections on the ratio of support radius and the mesh size (parameter κ). Square plate with central load.

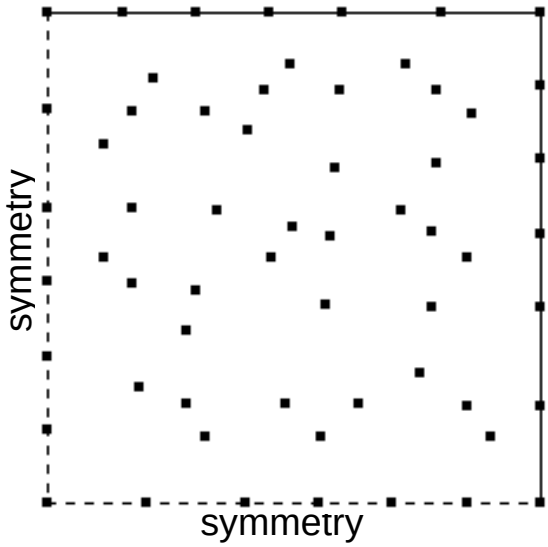

Figure 6: Irregular grid 7×7 on a quarter plate.

8.6 Convergence of displacements

The results plotted in graphs of this section were obtained for $\kappa = 3.9$, if not stated otherwise. Note, that in many cases the other "higher-accuracy" point $\kappa = 3.4$ could have given comparable results. The irregular grids in general require larger support radii to achieve good accuracy, however.

It can be noted that the results achieved by the EFG method are of good accuracy, especially when the lower number of displacement degrees of freedom (DOF's) is considered (actually, the finite element models with the same number of nodes have three times as many DOF's, because each node is associated to one deflection and two rotations).

The finite element results shown for comparison are due to: Jiroušek and Lan Guex [9] (triangle denoted HTT3) and Dhatt [7] (triangle denoted DKT). The reasons for this selection are: (i) both of them are of high accuracy, (ii) they represent two different approaches to the difficult problem of Kirchhoff plates – hybrid-Treftz (HTT3) and discrete Kirchhoff constraints (DKT).

The results for the simply-supported plate are summarized in figure 9, and those for the clamped plate are plotted in figure 10. The present results were tagged by "EFG xxx" with "F" meaning full plate model, and with "QR" and "QI" denoting the regular and irregular grid on quarter plate, respectively.

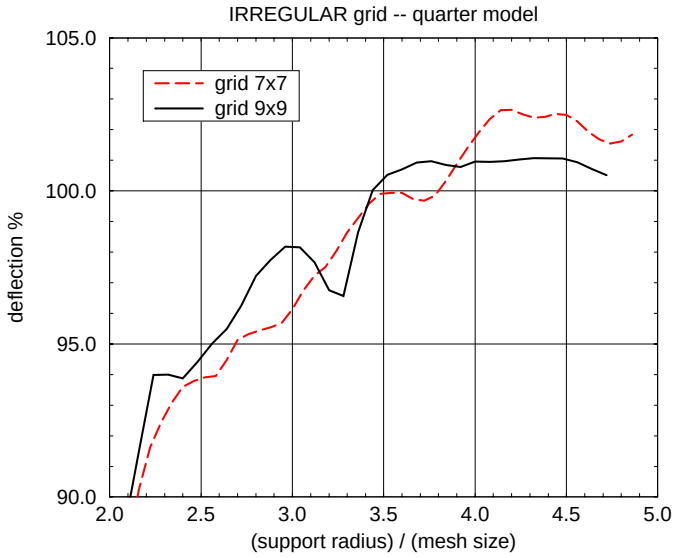

Figure 7: Dependency of the deflections on the ratio of support radius and the mesh size (parameter κ). Square simply-supported plate with central load. Irregular grids.

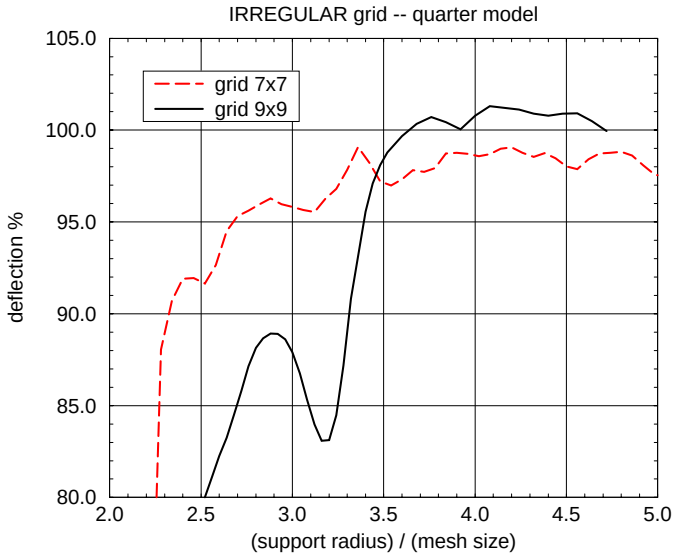

Figure 8: Dependency of the deflections on the ratio of support radius and the mesh size (parameter κ). Square clamped plate with central load. Irregular grids.

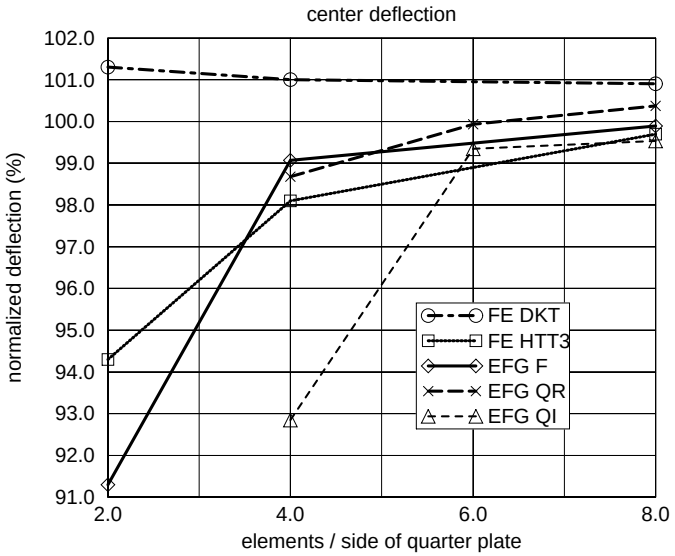

Figure 9: Convergence of deflection for the simply-supported square plate with central force.

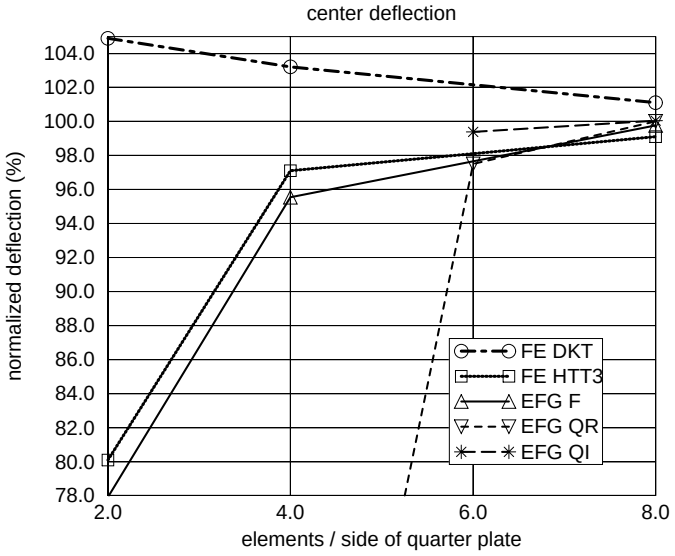

Figure 10: Convergence of deflection for the clamped square plate with central force.

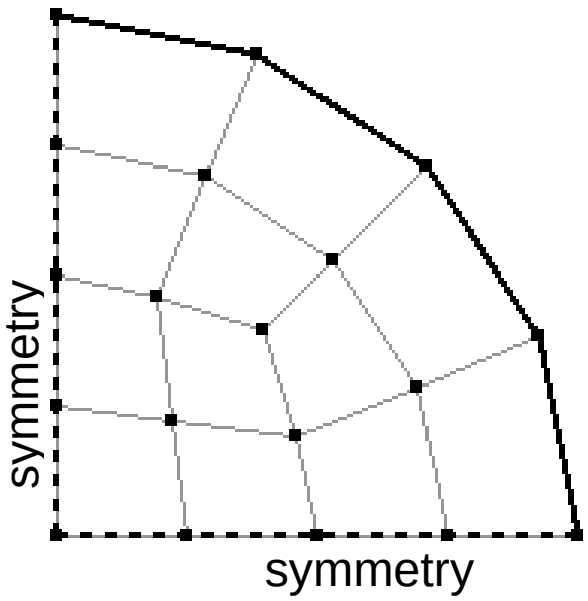

Figure 11: Regular grid of 19 EFG points on a quarter circular plate.

8.7 Circular plate

The problem analyzed is a circular clamped plate, with uniform transverse pressure $\bar{p}$. The analytic solution for thin, as well as for thick plates is available (*cf.* reference [5]). The deflection along the radial section is given for the thin plate case as

$$u_z(r) = \frac{\bar{p}}{64D}(R^2 - r^2)^2 \ ,$$

with R being the radius of the plate, t the thickness, and D the flexural rigidity of equation (2.6). The data values adopted for the present analysis were: $R = 1$, $t = 0.001$, $E = 10^9$, $\nu = 0.3$, $\bar{p} = 1$. The model consists of a quarter of the plate, using appropriate symmetry conditions.

8.7.1 Convergence in energy

The solution has been obtained for $K \times K \times K$ grids with $K = 4, 8, 12, 16$. The grids are quasi-regular in that the quadrangle shapes differ. They were generated from the first grid in figure 11 (filled circles stand for EFG nodes, the quadrature domains are drawn in lighter colors) by splitting the quadrilaterals appropriately, and by moving the EFG nodes on the exterior segments onto the exact circular boundary.

The normalized error in strain energy e is given as

$$e = \frac{\mathcal{E}_{exact} - \mathcal{E}_h}{\mathcal{E}_{exact}} \ ,$$

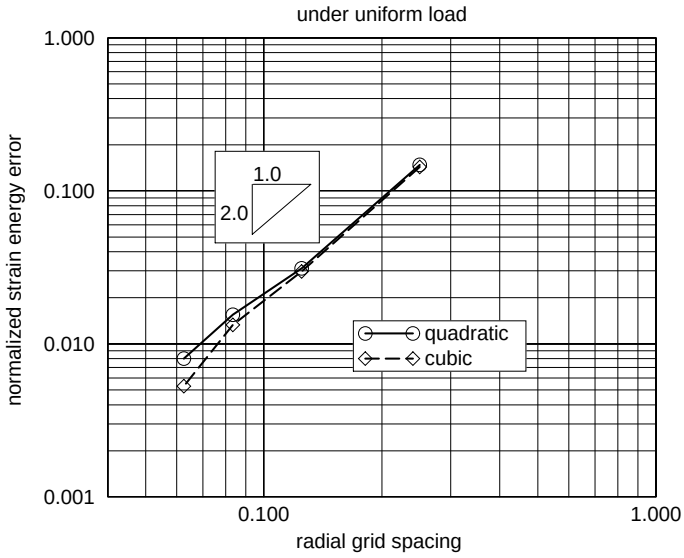

Figure 12: Strain energy convergence for the clamped, uniformly loaded, circular plate.

with $\mathcal{E}_{exact} = \pi\bar{p}^2R^6/(384D)$ the exact strain energy, and $\mathcal{E}_h$ the strain energy in the discrete system. The error e has been plotted in figure 12. The "mesh size" h has been set to R/K, with K being the grid parameter defined above (this is essentially the spacing of EFG nodes along the radial section). There are two plots in the figure – the first one corresponds to the quadratic polynomial basis p_j of equation (3.1), the second one is provided for comparison, and it was obtained for cubic polynomial basis (with x^3, x^2y, xy^2, y^3 as the additional terms). The slope of the plot is approximately 2.078 (least squares fit to all four results), and 1.94 respectively (least squares fit to last three results) for the quadratic basis, and approximately 2.379 for the cubic basis.

8.7.2 Influence of grid irregularity

The results were obtained for irregular grids generated from triangulations in the above described manner. One of the discretizations is shown in figure 13 (the filled squares are the EFG points).

The convergence of the center deflection was graphed in figure 14 in comparison with the DKT finite element [5] (the meshes used were *not* similar)x. The normalized results are plotted against the total number of degrees of freedom (i.e. the boundary conditions are disregarded for this purpose). The EFG results were computed for $\kappa \approx 4h$, where h is the fictitious grid size equal to 0.25 (grid 4×4), 0.2 (grid 5×5),

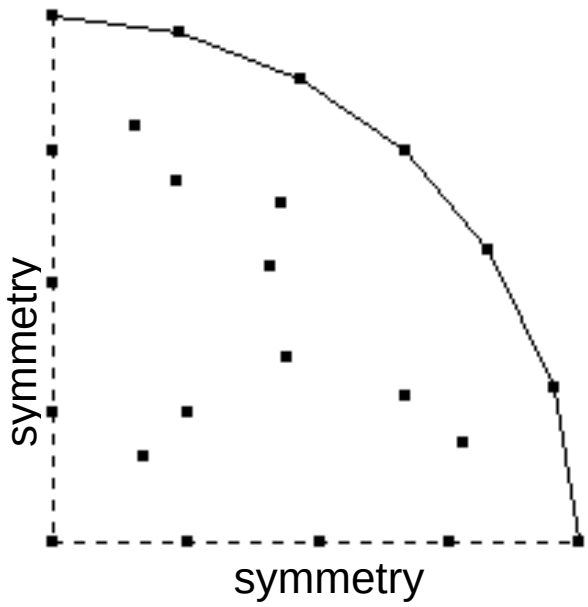

Figure 13: Irregular grid of 23 EFG points on a quarter circular plate.

0.1667 (grid 6×6), 0.125 (grid 8×8), and 0.1 (grid 10×10) for the five considered grids.

The results are of good accuracy, despite the fact that the grids are very irregular. Only the results for the smallest EFG grid are rather poor. This is so because of the insufficient number of DOF's in the whole model. Comparison with figure 2 shows that in the present EFG method approx. 40 EFG points are needed within the support to achieve good accuracy (for $\kappa \approx 4$), whereas the smallest grid had only 23 EFG points in total.

REMARK The non-monotonicity of the convergence in deflections is due to the grid irregularity.

9 Conclusions

The Element-Free Galerkin (EFG) method has been applied to thin (Kirchhoff) plates. Isotropic material law and uniform plate thickness were assumed for simplicity, the results apply directly to any material law and any thickness variation, however.

The domain is covered by a set of simple subdomains (background elements) for the purpose of numerical integration. Quadrilaterals were selected for the numerical implementation in this work, the geometric subdivision is immaterial, however,and

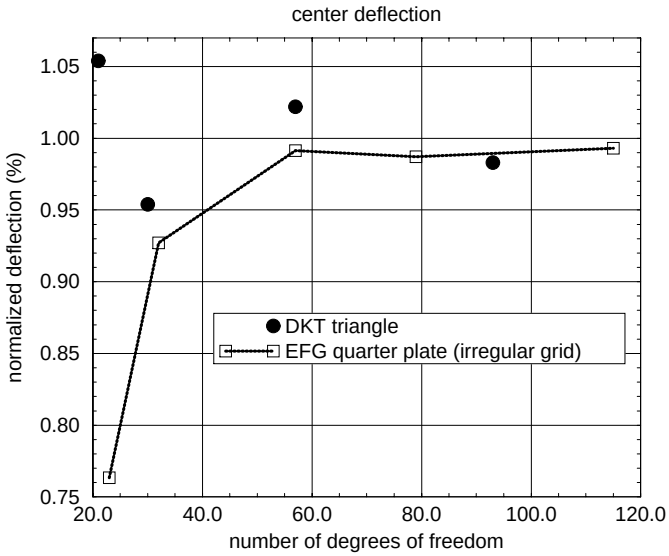

Figure 14: Convergence of deflection for the clamped circular plate under uniform transverse pressure with *irregular grids*.

any covering of the domain would do. The EFG nodes have been generated at the vertices of the geometric subdivision.

Numerical integration is carried out on the background elements by Gaussian quadrature. Numerical experiment to determine the optimal quadrature order has been carried out, with the result that a quadrature at 6×6 integration stations is close to optimal with respect to cost and accuracy.

The polynomial basis used is a complete polynomial of second degree in the spatial coordinates. Therefore, consistency is achieved automatically. The resulting approximation is governed by the continuity of the weight function, which was adopted as a quartic spline. This function possesses requested C^1 continuity within the support, as well as on its boundary. In fact, due to the properties of the quartic spline weight function of (7.2), C^2 shape functions are constructed. The implications are that smooth moments can be obtained without any re-interpolation or smoothing. Thus, while the finite element construction of C^1 numerical approximation is difficult and unsatisfactory so far, and while various devices to avoid the need for C^1 *ab initio* are employed (discrete Kirchhoff theory, hybrid stress, or even transition to C^0 theory), the current moving least squares method achieves C^1 approximation in a very straightforward manner.

The essential boundary conditions were enforced by Lagrange multipliers. One-point quadrature was applied along the spans between the EFG nodes on the supported boundaries. This is not the ideal method; however, more efficient and versatile techniques are under concurrent development.

The high accuracy and versatility of the present numerical approach have been

demonstrated on a number of examples: the square plate under a concentrated load (clamped and simply-supported), and the circular clamped plate for both regular and irregular uniform (i.e. not graded) grids. The EFG method is flexible with respect to the construction of the shape functions. Therefore, it is possible to optimize the accuracy of the method by the choice of the weight function, by the selection of the support of the EFG nodes (given by the weight function definition). A numerical study was presented, aimed at the selection of the support size. The support radius of approximately 3.9 of node spacings was discovered to yield good results for all the problems studied (for regular as well as irregular grids).

Acknowledgments

We gratefully acknowledge the support of the Office of Naval Research.

References

[1] T. Belytschko, L. Gu, and Y. Y. Lu. Fracture and crack growth by element-free Galerkin methods. *Modelling Simul. Mater. Sci. Eng.*, 2:519–534, 1994.

[2] T. Belytschko, Y. Y. Lu, and L. Gu. Element-free Galerkin methods. *International Journal of Numerical Methods in Engineering*, 37:229–256, 1994.

[3] T. Belytschko, D. Organ, and Y. Krongauz. A coupled finite element–element-free Galerkin method. *Computational Mechanics*, in press.

[4] J. Bunch, L. Kaufman, and B. Parlett. Decomposition of a symmetric matrix. *Numerische Mathematik*, 27:95–109, 1976.

[5] N. Carpenter, T. Belytschko, and H. Stolarski. Locking and shearing factors in C^0 bending elements. *Computers & Structures*, 22:39–52, 1986.

[6] W. S. Cleveland. *Visualizing data.* AT&T Bell Laboratories, Murray Hill, N.J., 1993.

[7] G. S. Dhatt. Numerical analysis of thin shells by curved triangular elements based on discrete Kirchhoff hypothesis. In Rowan W. R. and Hackett R. M., editors, *Proc. Symp. on Applications of FEM in Civil Engineering*, Nashville, Tennessee, 1969. Vanderbilt University.

[8] P. Hein. Diffuse element method applied to Kirchhoff plates. Technical report, Dept. Civil Engrg, Northwestern University, Evanston, Il., 1993.

[9] J. Jirousek and Lan Guex. The hybrid trefftz finite element model and its application to plate bending. *International Journal of Numerical Methods in Engineering*, 23:651–693, 1986.

[10] E. J. Kansa. Multiquadrics – a scattered data approximation scheme with applications to computational fluid dynamics: I. Surface approximations and partial derivative estimates. *Computers and Mathematics with Applications*, 19:127–145, 1990.

[11] E. J. Kansa. Multiquadrics – a scattered data approximation scheme with applications to computational fluid dynamics: II. Solutions to parabolic, hyperbolic and elliptic partial differential equations. *Computers and Mathematics with Applications*, 19:147–161, 1990.

[12] Y. Krongauz and T. Belytschko. Enforcement of essential boundary conditions in meshless approximations using finite elements. *Computer Methods in Applied Mechanics and Engineering, submitted.*, 1995.

[13] P. Lancaster and K. Salkauskas. *Curve and surface fitting: an introduction.* Academic Press, London, Orlando, 1986.

[14] T. Liszka. An interpolation method for irregular net of nodes. *International Journal of Numerical Methods in Engineering*, 20:1599–1612, 1984.

[15] W. K. Liu, Sukky Jun, S. Li, J. Adee, and T. Belytschko. Reproducing kernel particle methods for structural dynamics. *International Journal of Numerical Methods in Engineering, accepted for publication.*, 1995.

[16] Y. Y. Lu, T. Belytschko, and L. Gu. A new implementation of the element free Galerkin method. *Computer Methods in Applied Mechanics and Engineering*, 113:397–414, 1994.

[17] J. J. Monaghan. An introduction to SPH. *Computer Physics Communications*, 48:89–96, 1982.

[18] B. Nayroles, G. Touzot, and P. Villon. Generalizing the finite element method: diffuse approximation and diffuse elements. *Computational Mechanics*, 10:307–318, 1992.

[19] S. Qian and J. Weiss. Wavelet and the numerical solution of partial differential equations. *Journal of Computational Physics*, 106:155–175, 1993.

[20] W. G. Strang and G. J. Fix. *An analysis of the finite element method.* Prentice-Hall, Englewood Cliffs, N.J., 1973.

[21] S. Timoshenko and S. Woinowsky-Krieger. *Theory of plates and shells, 2d ed.* McGraw-Hill, New York, 1959.